





Article

Image Analysis Based Evaluation of Print Quality for Inkjet Printed Structures

Tim Horter ^{1,2}, Holger Ruehl ^{1,*} , Wenqi Yang ¹, Yu-Sheng Chiang ¹, Kerstin Glaeser ^{2,*} and André Zimmermann ^{1,2} 

¹ Institute for Micro Integration (IFM), Faculty 7—Engineering Design, Production Engineering and Automotive Engineering, University of Stuttgart, Allmandring 9b, 70569 Stuttgart, Germany

² Hahn-Schickard, Allmandring 9b, 70569 Stuttgart, Germany

* Correspondence: holger.ruehl@ifm.uni-stuttgart.de (H.R.); kerstin.glaeser@hahn-schickard.de (K.G.)

Abstract: Inkjet printing for printed electronics is a growing market due to its advantages, including scalability, various usable materials and its digital, pixel based layout design. An important quality factor is the wetting of the ink on the substrate. This article proposes a workflow to evaluate the print quality of specific layouts by means of image analysis. A self-developed image analysis software, which compares a mask with the actual layout, enables a pixel-based analysis of the wetting behavior by the implementation of two parameters called over- and underwetting rate. A comparison of actual and targeted track widths can be performed for the evaluation of different parameters, such as the tested plasma treatment, drop spacing (DS) and substrate temperature. To prove the functionality of the image analyses tool, the print quality of Au structures inkjet printed on cyclic olefin copolymer (COC) substrates was studied experimentally by varying the three previously mentioned parameters. The experimental results showed that the wetting behavior of Au ink deposited on COC substrates influences various line widths differently, leading to higher spreading for smaller line widths. The proposed workflow is suitable for identifying and evaluating multiple tested parameter variations and might be easily adopted for printers for in-process print quality control in industrial manufacturing.

Keywords: inkjet printing; digital printing; printed electronics; image processing; image analysis; wetting behavior



Citation: Horter, T.; Ruehl, H.; Yang, W.; Chiang, Y.-S.; Glaeser, K.; Zimmermann, A. Image Analysis Based Evaluation of Print Quality for Inkjet Printed Structures. *J. Manuf. Mater. Process.* **2023**, *7*, 20. <https://doi.org/10.3390/jmmp7010020>

Academic Editor: Steven Y. Liang

Received: 28 November 2022

Revised: 23 December 2022

Accepted: 3 January 2023

Published: 10 January 2023



Copyright: © 2023 by the authors. Licensee MDPI, Basel, Switzerland. This article is an open access article distributed under the terms and conditions of the Creative Commons Attribution (CC BY) license (<https://creativecommons.org/licenses/by/4.0/>).

1. Introduction

Printed electronics is a growing market with many applications such as display technology, photovoltaics, antennas and sensors, e.g., for bio applications [1–3]. One manufacturing technology in those fields with many advantages is inkjet printing. It is a digital process that enables individual, scalable deposition of various inks and materials such as Au, Ag, conductive polymers and insulating materials on different substrates such as polymers, ceramics or glass. Piezo based drop-on-demand inkjet systems are mostly used in printed electronics because they allow a pixel based layout design. This enables resource-friendly manufacturing processes since the precious functional materials are only deposited where they are needed.

The printing quality of the structure and the later performance depend very strongly on the ink setting on the substrate and are influenced by a variety of different parameters. Conditions before the actual manufacturing, like, for example, cleaning procedures, ink composition, plasma activation for polymers and other surface modifications, influence the wetting behavior. Printing parameters such as drop spacing, drop ejection, print direction, layout design and drying can influence the print quality to create line widths down to 50 µm [4]. With regard to printed electronics, knowing exactly how the ink wets a substrate surface is crucial. The unpredicted flow of conductive ink, such as overwetting, can result in shortages or, in the case of underwetting, unwanted behavior, such as resistance changes or

insufficient current carrying capacity. Finding suitable parameters is mostly only applicable to specific material combinations and requires manual tests [5].

An often-used method to influence wetting is to adjust the ink's properties, e.g., by adding solvents and surfactants and to determine their influence by contact angle measurements as conducted in [6,7] or [8]. To minimize testing efforts, [9] implemented a jetting prediction tool to improve jetting capabilities of newly formulated inks. Other approaches, such as [10], tried to improve the wetting by surface treatment with plasma or excimer laser treatment [11]. Contact angle measurements, in general, can only show better or worse wetting. Specific inkjet manufacturing influences such as the very low droplet volume in the picoliter range, effects of droplet speed and impact or interactions with already deposited ink cannot be included in these measurements. An interesting approach to increase the understanding of (multiple) droplet(s)/surface interaction in inkjet printing by means of simulation methods was established in [12]. This reference shows a first step towards the simulation of single line printing and how surface treatment can influence line quality and concludes that a 30–40° contact angle is most suitable to print a single line.

One way to improve the overall printing quality is the implementation and tracking of quality factors by the use of image analysis. Bischoff et al. [13] implemented a test bench for the evaluation of new inks and for acquiring print quality data such as size, shape and centroid position of single droplets on a substrate. The setup consists of a printhead, fluorescence and color cameras for quality control with LED illumination and a drop watching station. Droplet positions were converted into a binary mask for further algorithmic evaluation. An alternative technique to improve the printing quality for complex layouts (layouts containing multi-lines, crossings, junctions or multilayer systems) is the implementation of design kits by optical evaluation [14–16], showing the problems of such layouts and using pattern compensation as a possible solution for the specific ink/substrate combinations. A method to create a design kit for inkjet printing of a 4-layer (metal, dielectric, metal, and organic semiconductor) design is displayed in [17]. Layout features such as line width, spacing, corner distances and overlapping can be evaluated electrically and optically. However, the features were only characterized as good/bad, but no quantitative values were detected. With regard to creating a design kit, [18] went one step further and suggested a method to adjust the layout to bitmap conversion with the extracted design rules. Ref. [19] improved this method by the use of machine vision and image extraction technologies to automatically detect failures in printed structures and adjust layouts and printing parameters such as drop sequence accordingly. In order to achieve such results, a single nozzle inkjet printer was modified with a strobe light and camera to detect the ejected single droplets. In [20], a design kit for hybrid electronics (printing, sintering and SMD mounting) is discussed. With the implementation of complex machine and image processing methods, a system for simple hybrid electronics was created. All of the above-mentioned references [11–18] used image processing and analysis tools to gain data for an adjustment of the printing process in order to increase the printing quality. Most of them require technically complex printers and special tools, which are not applicable for printing complex layouts with multiple nozzles. In addition, some do not take the effects of wetting behavior or the interaction between substrate and ink into account.

In this paper, a simple workflow using a self-developed image analysis tool to find suitable surface pre-treatment and printing parameters to achieve good print quality is proposed. The workflow, shown in Figure 1, consists of

1. inkjet printing of a specific test layout,
2. microscope imaging,
3. image analysis to assess the print quality and
4. finally, a manual determination to optimize the pre-treatment and printing parameters.

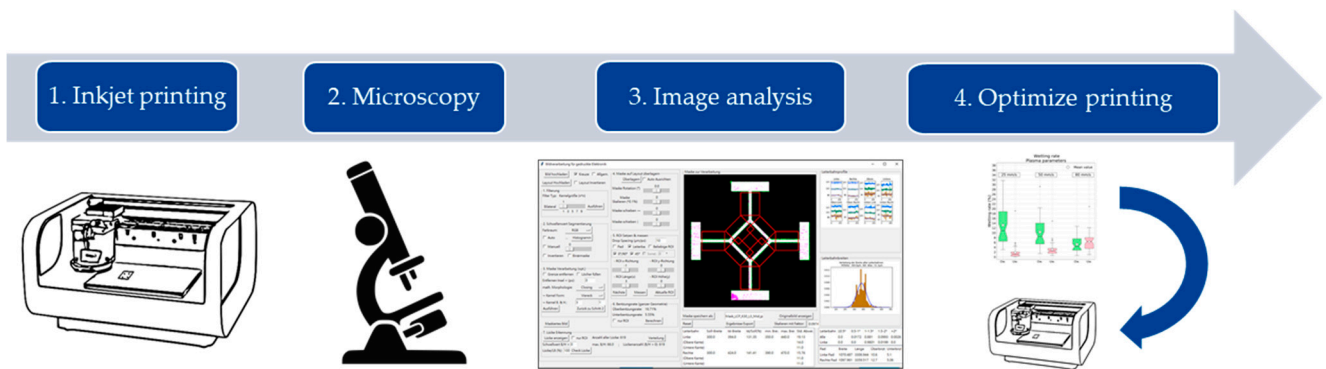


Figure 1. Workflow for improving the print quality in inkjet printing based on an image analysis evaluation.

To demonstrate the functionality of the proposed workflow, Au ink was inkjet printed on COC, a substrate/ink combination that has proven useful for medical applications, as shown in [1] and [21]. The workflow might be easily adopted for different printers and for different substrate/ink combinations. It may also be used as a first step for design kits and for quality control in industrial production.

2. Materials and Methods

2.1. Experimental Design for Printing

The functionality of the workflow was tested for a given substrate material and ink by analyzing a set of plasma speeds, drop spacing and substrate temperatures in order to find the most suitable printing parameters for sufficient print quality. Every parameter set contained fixed parameters, which were either predetermined or determined based on the image analysis conducted in the previous investigation step. The schematic experimental process, including the fixed and varied parameters, is shown in Figure 2. The parameters to be determined in the previous investigations are highlighted by a question mark. To begin with, the plasma speed was varied by already existing treatment programs containing the same distance to the substrate. In the following investigation, the drop spacing was varied for a predetermined substrate temperature and the plasma speed, determined in the previous investigation. Last, the substrate temperature was varied between 50 °C, 55 °C and 60 °C for the plasma speed and drop spacing gained in the steps before.

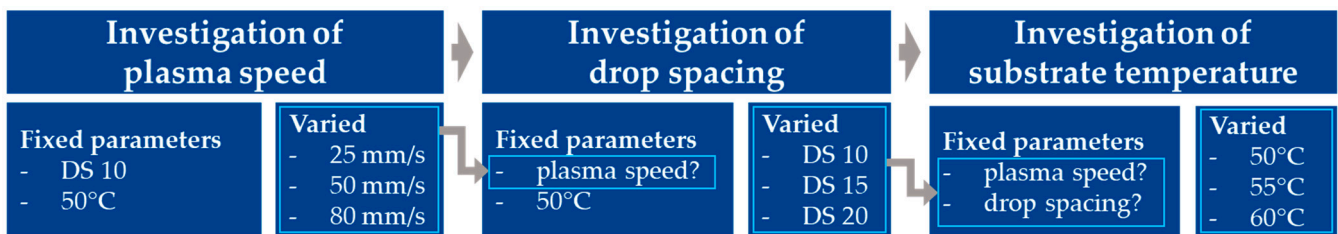


Figure 2. Schematic process parameter sets for inkjet printing experiments.

2.1.1. Materials and Pretreatment

Injection-molded plates from COC 5013 S-04 from Topas Advanced Polymers GmbH, Raunheim, Germany, were used as substrate material. Drycure Au-J 1010B from C-INK Co., Ltd., Soja City, Japan, was used as ink. The ink formulation and properties are provided in Table 1. For the surface tension, both the manufacturer specifications and a measured value from [10] are given. Pretests were conducted on liquid crystal polymer (LCP) Vectra E840i LDS from Celanese, Irving USA, with silver nanoparticle ink I-30EG1 from PV Nanocell Ltd., Migdal Ha’Emek, Israel. Prior to further processing steps, all substrates

were ultrasonically cleaned with isopropanol for 3 min, rinsed with distilled water and then dried in a furnace for one hour at 80 °C.

Table 1. Formulation and properties of Drycure Au J 1010B (C-INK CO, Ltd., Soja City, Japan) [10,22,23].

Parameters [Unit] (Measuring Condition)	Au J 1010B
Ink composition [wt%]	Au content concentration 10/ water and additives 90
Viscosity [mPA s] (25 °C)	10
Surface tension [mN/m] (dispersive/polar share)	30 32.6 (28.4/4.2)
Metal particle size [nm]	15–20
Volume resistivity [Ωcm]	5×10^{-5}

COC substrates have to be plasma activated for inkjet printing with Drycure Au J 1010B due to their low surface energy [1]. An atmospheric plasma system FG5001 equipped with a rotation nozzle RD1004 from Plasmatreat GmbH, Steinhagen, Germany, was used. The varied parameter for the activation was the traversing speed with 25 mm/s, 50 mm/s and 80 mm/s. The distance between the nozzle and the substrate, as well as the plasma generator, was kept constant.

2.1.2. Printing

Inkjet printing was conducted with a Dimatix DMP 2850 from Fujifilm Dimatix, Inc. Santa Clara, CA, USA, in a clean room facility with Samba 2,4 pl cartridges, specified in Table 2. The printing equipment allows the use of 12 firing nozzles, but only two nozzles were used in the experiments to establish the same drying parameters for each tested parameter set and to allow a stable printing process. The DMP 2850 printer allows the heating of substrates from 28 °C up to 60 °C. The experiments were performed at 50 °C, 55 °C and 60 °C, respectively. For each parameter set, three substrates were produced with one printed ink layer at the same parameters to establish a certain statistical background for the experiments.

Table 2. Specification of the printer and cartridges used in this study [24,25].

Specifications		
Printer	Printable area (substrate size x thickness [mm])	210 × 260 × 25
	Substrate holder temperature [°C]	28 to 60
Cartridge	Nozzles	12
	drop size [pL]	2.4–10.0
	Native resolution [DPI]	75
	Jetting frequency [kHz]	max. 15
	Achievable dot size [µm]	30

Drop spacing is defined by the pixel size within the layout as well as the cartridge angle of the printer and determines the distance between the center point of each droplet [26]. In the experiments, 10 µm, 15 µm and 20 µm DS were tested to ensure overlap between each drop.

The printing layout and its features are displayed in Figure 3. It consists of four crosses with trace widths of 100 µm (L1), 300 µm (L3), 500 µm (L5) and 800 µm (L8). Each cross contains traces in the directions 0°, 45°, 90° and 135° to the print direction. In addition, each cross was surrounded by four pads, respectively. The size of the pads was 1000 µm × 4000 µm. These pads are used not only to characterize the wettability but also as alignment markers to position the geometry during image processing precisely.

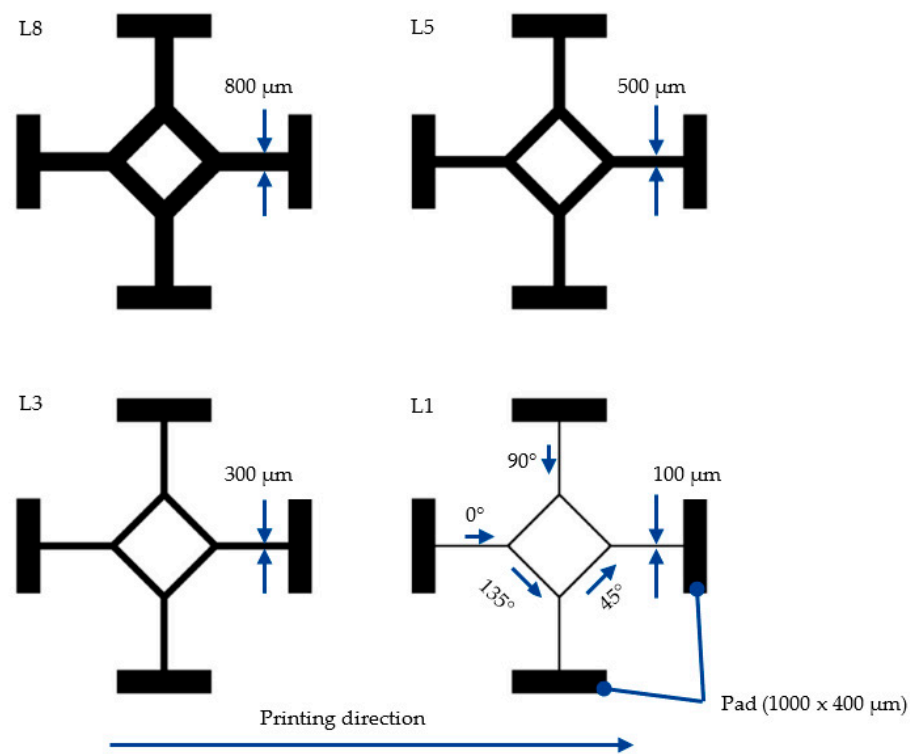


Figure 3. Printing layout design with labeled trace widths 100 μm (L1), 300 μm (L3), 500 μm (L5) and 800 μm (L8), traces twisted 0°, 45°, 90° and 135° to the printing direction and pads.

2.2. Microscope Imaging and Image Analysis

The images for the subsequent analysis were taken with an SMZ 1270 stereomicroscope from Nikon, Minato, Japan, with the illumination device KL 1500 LCD from Schott, Mainz, Germany and a white background. The image was taken in that specific setup to avoid shadows due to high-profile changes and reflections from the substrate surface captured.

The software for image analysis was programmed in python using opencv and tinker for image manipulation and user interface. The analyzing sequence within the software tool is displayed in Figure 4, beginning with the import of both the original layout and the microscope image, followed by the mask creation (Section 2.2.1) and the mask and layout overlay (Section 2.2.2). In the last step, the definition of the region of interest (ROI) and a quality assessment was executed (Section 2.2.3). Mask creation can be adjusted to fit the needs of different substrate/ink combinations and to improve the image quality for analysis.

2.2.1. Mask Creation

After the image import, the user can manipulate the image with preselected filters such as Gaussian, mean value, median, and bilateral filtering and choose a convolution kernel size to determine the effect of the filter. This allows noise reduction (denoising) in the images. Noise in a digital image is a random variation of information such as brightness and color and, therefore, mostly a deterioration of the image [27–30].

For the printed samples on COC 5013 S-04, the bilateral filter with a convolution kernel size of 3 pixels provided the best fit among the available filters and was therefore chosen. Other substrate/ink images might need other filtering parameters.

Converting the image from RGB to a binary image was conducted by means of thresholding to create a mask of the printed structure. This conversion was necessary because of the needed separation of the printed structure (foreground) from the substrate (background) to extract features for analysis. Separation was conducted by setting a defined value in a histogram for each image depending on its specific characteristics. To determine

the threshold value for various ink/substrate combinations, different thresholding methods are available to the user. The user can choose between the options “Greyscale”, “brightness” and “saturation” thresholding. “Greyscale” conversion determines the threshold value based on light intensity. “Brightness” and “saturation” thresholding methods originate from the hue/saturation/value (HSV) color space. For image processing, the brightness value and the saturation are the commonly used parameters to determine the contrast between foreground and background [31]. The threshold value can either be determined manually with a displayed histogram or by an automatic procedure called Otsu-method. The Otsu-method is a variance method to select values within and between different classes [32]. Within a class, the variance should be as low as possible. Between the classes, the variance should be as high as possible.

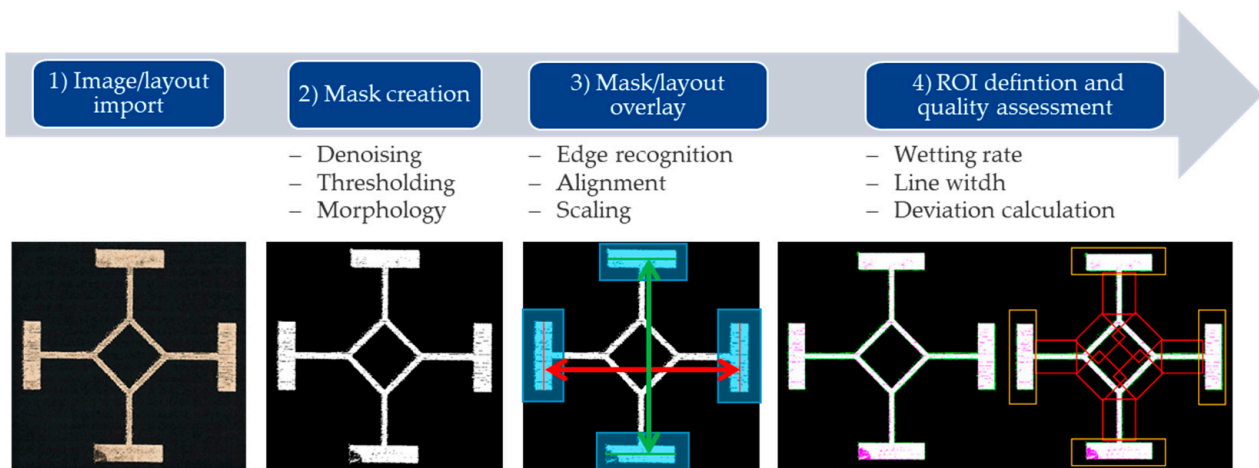


Figure 4. Analyzing sequence within the image analysis tool comprising the steps (1) image and layout import, (2) mask creation (Section 2.2.1), (3) overlay of mask and layout (Section 2.2.2) and (4) the definition of the region of interest and final quality assessment (Section 2.2.3).

For the COC substrates with printed Au ink structures, the later described evaluation of the printing experiments was performed by automatic thresholding with the brightness option.

Some masks need further optimization because they contain bad information, such as droplet splashes or image shadows on the printed structure, which are wrongfully displayed as background. The software tool, therefore, offers several options, such as “island detection”, which eliminates single droplets with a manually defined pixel size. A useful tool is the use of mathematical morphology to simplify images by preserving essential shape features of objects and eliminating irrelevant objects [33]. By use of a convolution kernel, there are two basic operations available: erosion and dilatation. With erosion, the kernel is always erased, and with dilatation, it is always filled. “Opening” and “closing” are mathematical morphology operations based on erosion and dilatation. The opening is defined as erosion before dilatation, and closing is dilatation and afterward an erosion operation [34]. In combination with the specific kernel size (namely: rectangle, ellipse and cross), the mask quality can be significantly increased. An example is given in Figure 5 for Ag ink on an LCP substrate. Figure 5a shows the original image with some shadows from the microscope’s illumination on the printed structure due to surface inhomogeneity. Figure 5b shows the mask after thresholding, and Figure 5c shows the improved mask. The improved mask matches better with the original image and only displays the underwetting areas and not the shadows.

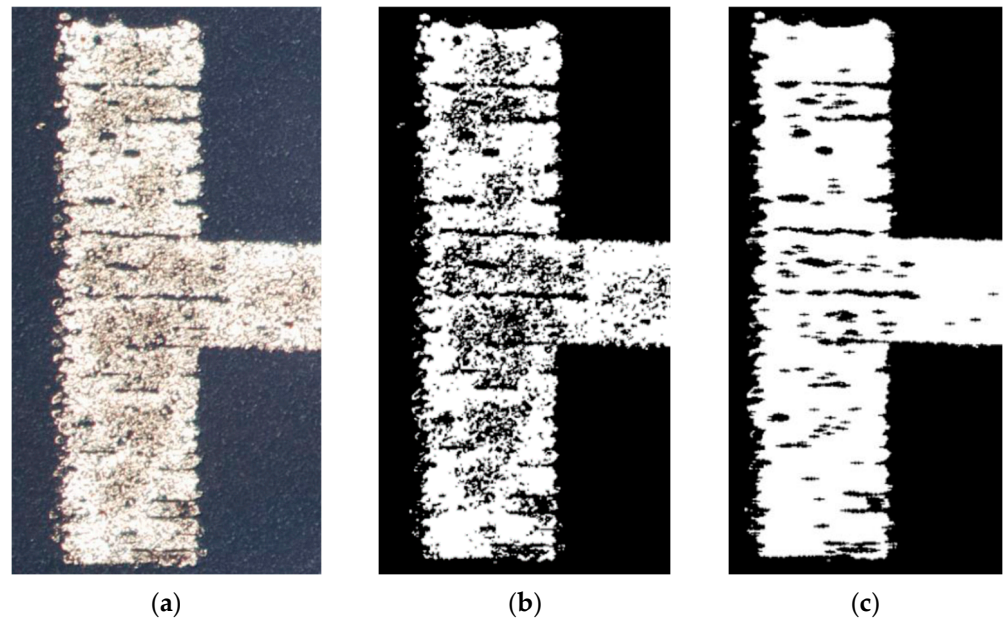


Figure 5. Example of closing specific gaps using “closing”: (a) A sample from the LCP substrate with poor print quality, (b) the basic mask using the thresholding method and (c) closing with an elliptical kernel ($a = 11, b = 3$).

For the COC substrates with printed Au ink structures, a morphology operation was not needed and, therefore, not conducted.

2.2.2. Mask/Layout Overlay

Mask/layout overlay is an automatic feature for the specifically designed layout. In order to analyze the microscopy image, the pixel to micrometer ratio must be known. For some images, this is not the case. Hence, a scaling procedure was implemented, which uses edge recognition of the four pads and calculates a middle line for each pad. Those middle lines can be used to determine the rotation angle, width, height, and center of gravity for the printed structure. By calculating those values for the mask and the layout, a scaling factor can be determined to resize the mask to the layout dimensions. Overlaying the mask and layout was achieved by aligning the two centers and rotating the images by the determined rotation angle.

This overlay leads to a pixel based comparison of areas in which ink is not present as specified (underwetting) and areas in which ink should not be present (overwetting). Figure 6 shows examples of two printed structures, (a) for large underwetting areas and (b) for large overwetting areas.

2.2.3. ROI Definition and Quality Assessment

For the layout image, the pixel to micrometer ratio is known because it is needed for printing. Due to the scaling procedure, the mask and layout have the same resolution. This allows a detailed analysis of wetting rates, pad geometry, track widths, track width deviation and track edge quality. The total wetting rate is defined as the underwetting rate (1) and overwetting rate (2) as follows:

$$\text{underwetting rate (uw.)} = \frac{\text{pixelcount magenta in Figure 6 (a)}}{\text{pixel count of layout}} \tag{1}$$

$$\text{overwetting rate (ow.)} = \frac{\text{pixelcount green in Figure 6 (b)}}{\text{pixel count of layout}} \tag{2}$$

These wetting rates indicate the wetting behavior of the whole layout for a specific drop spacing and a specific track width. If layouts with different track widths are to be

compared, it is best to use the ROI feature for the pads to always compare the same amount of pixels. By specifying certain ROIs for pads and tracks, their widths can be evaluated as mean value with standard deviation, actual/target comparison and minimal value. Because this evaluation is based on the edge recognition feature, it is also possible to calculate a mean value with standard deviation for each edge of a track and therefore evaluate the spreading and the line quality. The ROI evaluation tools allow separate evaluation of all tracks with 0° and 90° orientation, tracks with 45° and 135° orientation, all pads or a single, user-defined rectangle for analysis. Defining the rectangle-shaped ROI was conducted manually to allow the user to exclude certain features to obtain a defined and comparable result. For the results in the following chapters, the pad wetting rates and actual/target comparison of track width, regardless of their orientation, are compared.

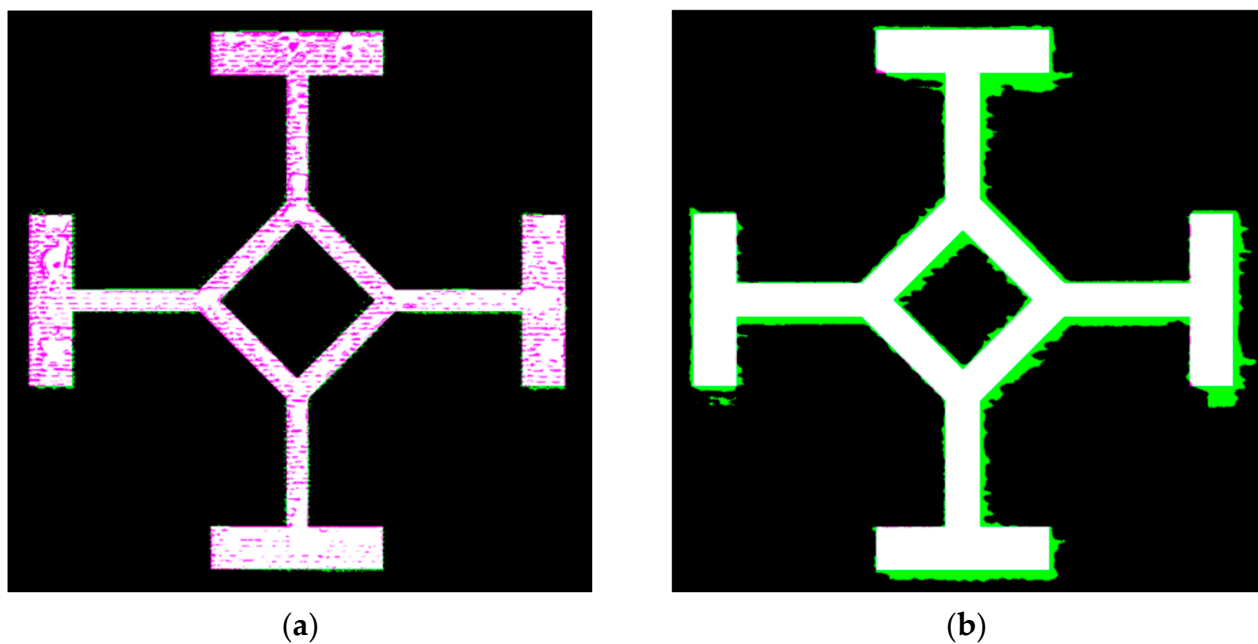


Figure 6. Examples for underwetting (a) displayed in magenta areas and overwetting (b) displayed in green areas.

3. Results

For the previously described methods and experimental setup, the following results were achieved. Wetting rates and actual/target comparison of track widths were evaluated to determine the influence of each varied parameter set and the most suitable parameters for the analyzed ink/substrate combination. Other parameters to determine the printing quality, such as particle distribution and resistance, are not explicitly analyzed but are briefly discussed where necessary.

3.1. Plasma Speed

Different plasma speeds were tested and analyzed according to their wetting rate, in detail, overwetting and underwetting rate, as shown in Figure 7. The plasma speeds were varied from 25 mm/s to 50 mm/s and 80 mm/s by DS 10 and a substrate temperature of 50°C as fixed parameters. Increasing the plasma speed leads to shorter exposure times of the substrate and, therefore, may lead to a different wetting behavior. Figure 8 shows the results in a boxplot diagram.

Investigation of plasma speed	
Fixed parameters	Varied
- DS 10	- 25 mm/s
- 50°C	- 50 mm/s
	- 80 mm/s

Figure 7. Fixed and varied process parameters for the investigation of plasma speed.

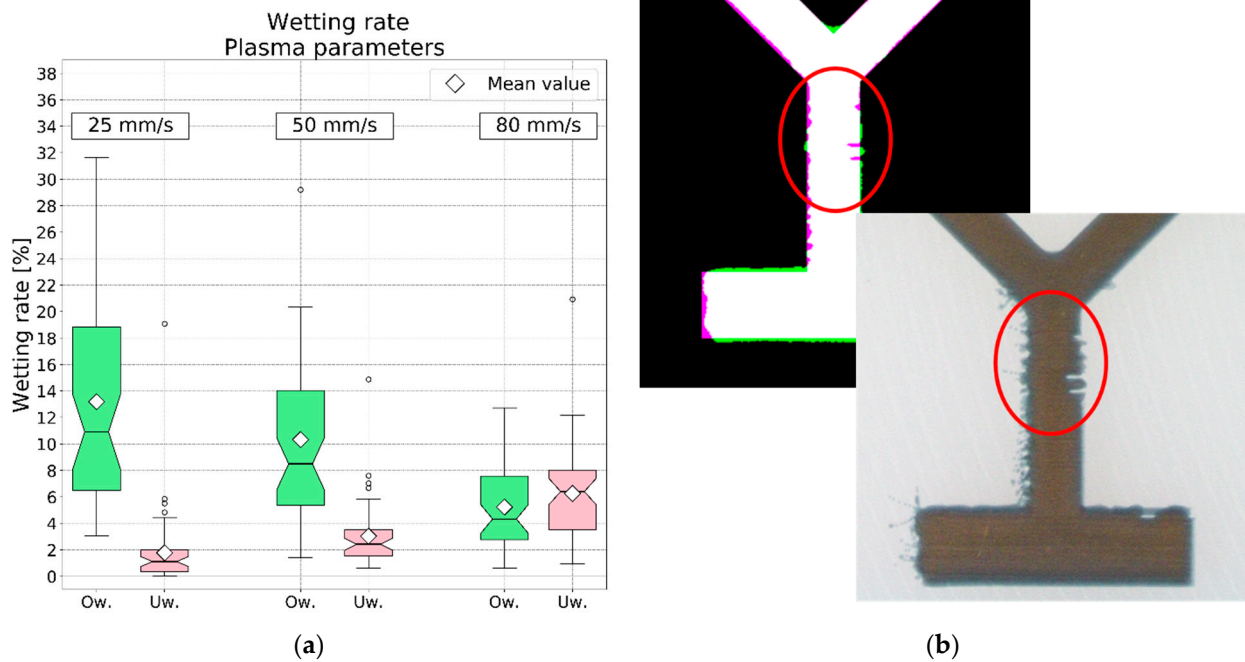


Figure 8. (a) Box plot diagram of wetting rates including overwetting (Ow.) and underwetting (Uw.) by varied plasma parameters (b) Example of a 50 mm/s treated L8 sample displaying function critical narrowing inside the red circles.

By comparing the mean values of the wetting rates, an almost linear trend can be seen between treatment times and wetting influence. In comparison to the other ow values, the relatively high overwetting rate at 25 mm/s with a mean value of about 13% is to be neglected since both 25 mm/s and 50 mm/s exhibit large ranges of overwetting rates.

For a plasma speed of 50 mm/s, an underwetting rate with a mean value of about 3% was determined (see Figure 8a), which means a decrease of track width of approx. 22%. Since high underwetting can lead to function critical narrowing (see Figure 8b) or shortages, the lowest underwetting rate at 25 mm/s should be preferred to 50 mm/s or 80 mm/s.

3.2. Drop Spacing

The best parameters from Section 3.1 (25 mm/s, DS 10 and 50 °C) show a relatively high overwetting rate. As given in Figure 9, the plasma speed of 25 mm/s and substrate temperature of 50 °C were therefore set as fixed parameters for the investigation of the drop spacing. By increasing the drop spacing, less amount of ink is printed on the substrate. Thus, overwetting might be diminished since less ink needs less time to dry and, therefore, cannot spread too wide.

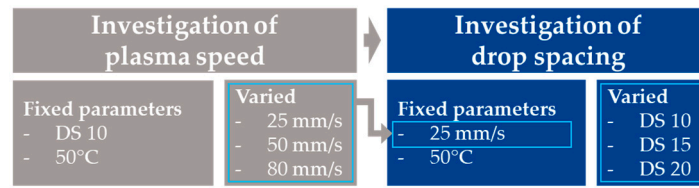


Figure 9. Fixed and varied process parameters for the investigation of drop spacing.

Results of wetting rate for increased drop spacings of 10 μm , 15 μm and 20 μm in Figure 10a show that DS 20 leads to a significantly decreased ow while increasing underwetting to a not usable rate. Underwetting for DS 10 and DS 15 is almost comparable; although the mean value is reduced from 1.78% to 1.00%, the range and the outliers are in the same magnitude. Doubling the drop spacing from DS 10 to DS 20 does not lead to a halved overwetting rate, so there is no linear correlation between drop spacing and wetting. DS 15 has a mean ow rate of about 13%, but in contrast to DS 10, it exhibits a much smaller value range with an almost symmetrical normal distribution since the mean and median values are about the same [35]. This could mean that the user can use this parameter set to design layouts where the risk of short circuits between individual traces is minimized.

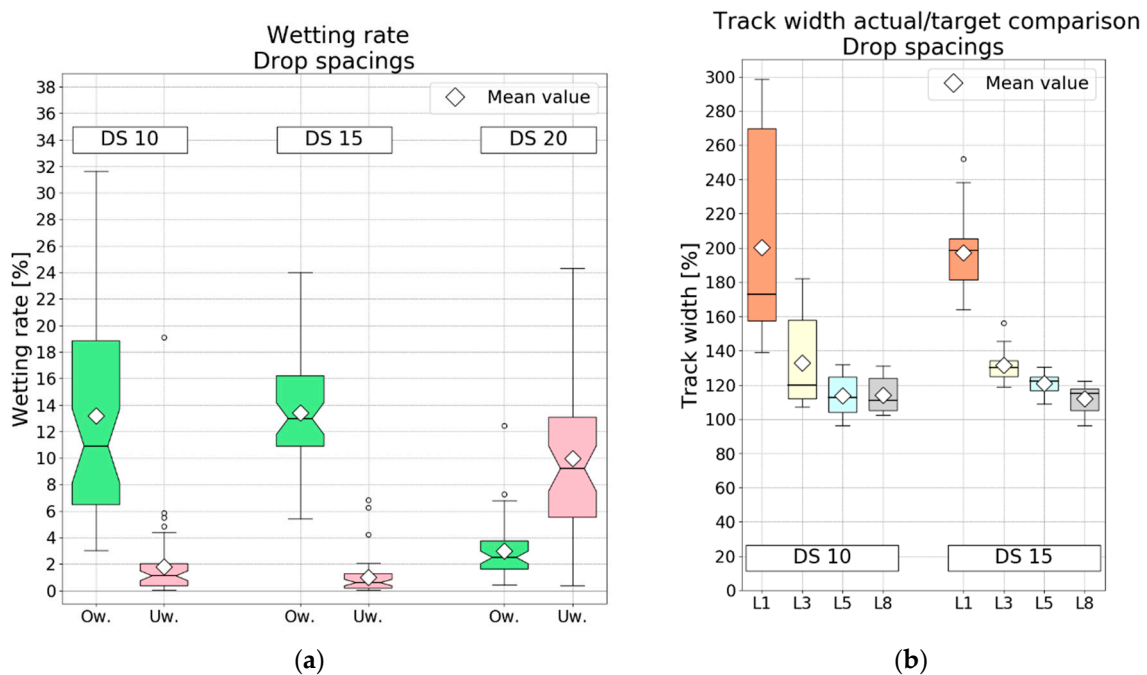


Figure 10. Boxplot diagrams of (a) Wetting rates, including overwetting and underwetting and (b) track width actual/target comparison for different line widths by varied drop spacings.

How this fact actually transfers to specific layout designs and track widths is displayed in Figure 10b by the actual/target comparison of the different track widths for DS 10 and DS 15. Both parameters show an almost identical magnitude of spreading values, such as the doubling in actual track width for L1 (100 μm track width). Wider tracks such as L3, L5 and L8 reduce the spreading and the range of the track width for each parameter set significantly. This shows the user that track widths below 300 μm can only be used with significant obstacles, such as high pitch and uncontrollable ink spreading in layouts. In comparison from DS 10 to DS 15, DS 15 track widths have a very low interquartile range (IQR), which describes the difference between the first and third quartiles of data. Since DS 15 provides, therefore, a far better line quality with an almost symmetrical value distribution, DS 15 was the better choice for further testing in the following investigation of the substrate temperature.

3.3. Substrate Temperature

The last tested parameter set was the substrate temperature. With the parameters for the plasma treatment of 25 mm/s and a drop spacing of 15 μm found in the previous analyses, the substrate temperatures of 50 °C, 55 °C and 60 °C were evaluated, as shown in Figure 11. Higher substrate temperatures normally increase the drying and, therefore, could control the spreading of the ink, which may result in better line quality.

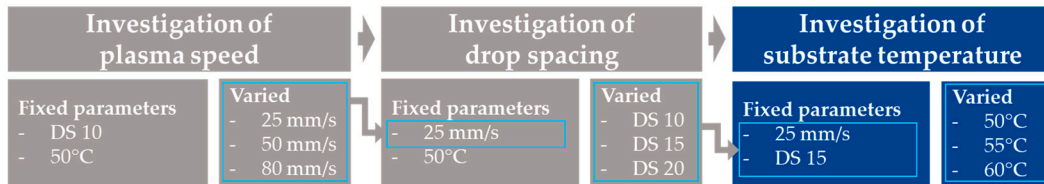


Figure 11. Fixed and varied process parameters for the investigation of substrate temperature.

Analyzing the wetting rates in Figure 12a, a clear reduction of overwetting rates can be noticed with increasing temperature, while the ranges stay comparable. Since ow. for 55 °C and 60 °C due to their similar mean, median and IQR are the same and underwetting actually increases for 55 °C and then decreases again for 60 °C, no linear correlation for substrate temperature and wetting behavior can be concluded.

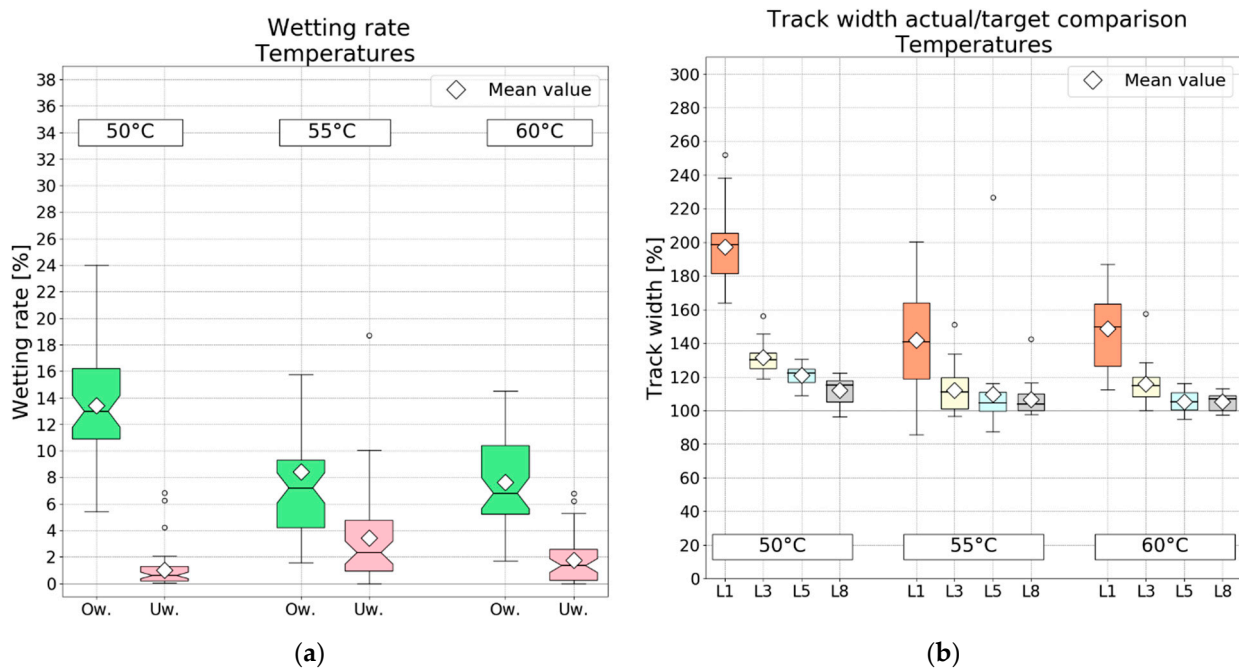


Figure 12. Boxplot diagrams of (a) Wetting rates, including overwetting and underwetting and (b) track width actual/target comparison for different line widths with varying substrate temperatures.

Further analysis of substrate temperatures by means of actual/target comparison shows that an increase in temperature also leads to much lower spreading of tracks. L3 values ranges are both reduced under 120% of spreading, while L1 mean values are below the acceptable threshold of <150%. Higher IQRs for L1 and L3 at 55 °C and 60 °C may be due to the higher underwetting rate and its greater influence on small features for these parameters.

This effect could be explained by comparing the actual images of the printed structures in Figure 13a,b. While the 50 °C sample exhibits a closed homogeneous surface with some overwetting effects on the track edges, the 60 °C sample shows straight track edges but

exhibits areas with an inhomogeneous particle distribution. These areas may still achieve some conductivity, but the whole track will not have the same resistance and the same current carrying capacity. This could be validated by an exemplary resistance measurement, which showed about four times higher resistance for a 60 °C sample compared to a 50 °C sample. Since the inhomogeneous particle distribution is tracked by the image analysis tool due to the displayed color difference of these areas, both the underwetting rate and IQR for L1 and L3 are higher for temperatures of 55 °C and 60 °C. With regard to L8 values, it may be possible that the increased amount of ink leads to a better particle distribution at higher temperatures.

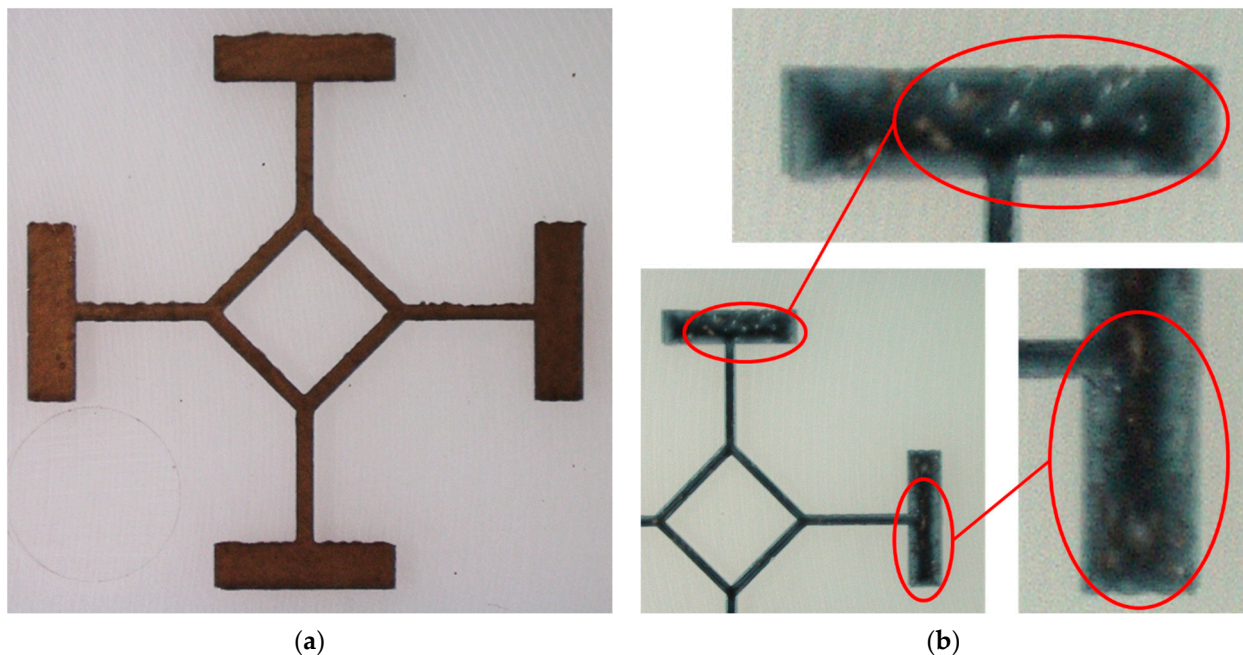


Figure 13. L3 probes for a substrate temperature of (a) 50 °C and (b) 60 °C.

One possible solution to fill areas with less particles is the printing of multiple layers. As the ink in the experiments has a comparable low particle load of 10% and most applications require high conductivity anyways, multiple layers are an application-oriented approach. The analysis of a single sample with four layers shows the tendency of improving surface homogeneity with a lower underwetting rate while increasing overwetting. With regard to the spreading of the tracks, a slightly higher spreading could be noticed.

4. Discussion and Conclusions

This article proposes a simple workflow based on image analysis, which could be used to evaluate the print quality by quantifying the wetting behavior of inks deposited on substrates by inkjet printing. The described process consists of inkjet printing of a specific layout, optical analysis using microscopy, image analysis of inkjet printed structures using self-developed software and a final evaluation method to determine the optimal printing parameters manually.

The functionality of the workflow was demonstrated by inkjet printing a single layer of Au ink on COC, followed by an analysis of different wetting rates and, where necessary, track widths for different plasma treatments, drop spacings and substrate temperatures. The finally found parameters are a plasma treatment with a traversing speed of 25 mm/s, a drop spacing of 15 μm and a substrate temperature of 60 °C. The analysis of the measured wetting rates shows a nearly linear influence of varied parameters for different plasma treatments. Changing the drying of the ink by influencing ink amount (DS) or substrate temperature can further improve the wetting once a suitable plasma parameter is established. For

the tested drying parameters, using the next possible drop spacing improves the wetting behavior only by reducing the IQR of overwetting from 12.4% (DS 10) to 5.3% (DS 15) and not the level of the wetting rates themselves. Therefore, a more stable process is established. However, increasing the substrate temperature from 50 °C to 60 °C does not improve the IQR for the overwetting rate but decreases the mean value from 13.4% to 7.4%. The underwetting slightly increases from 1.00% to 1.7% with an IQR rise from 1.1% to 2.3% and is still in an acceptable range, as track widths do not drop below their target widths. These results make the substrate temperature a powerful parameter to improve the wetting for the tested Au ink on COC. With regard to the track width, 800 µm and 500 µm wide tracks show the least spreading, about 100–110%, while smaller track widths exhibit wider spreading (300 µm of about 110–120% and 100 µm even up to about 130–165%). Hence, the established final parameters are not ideal for smaller track widths.

Almost all of the measured values, in comparison to their absolute value, show high IQRs, especially for smaller track widths. This may be a sign of not ideal droplet placement since the effect rises at smaller feature sizes and improves on larger areas, where a single drop does not influence the whole structure in the same amount. The established workflow could therefore be used as an indirect measurement technique for drop placement. Improvements in drop placement, such as optimizing waveform, firing voltage, nozzle conditions, firing frequency or nozzle temperature, could lead to smaller IQR values for the evaluated structures.

The gained final parameters are only to be seen as the geometrically best fit parameters regardless of the structure's actual resistance values. As already mentioned in Section 3.3, particle distribution and, therefore, the resistance and the current carrying capacity are critical features in printed electronics. Preliminary tests show a possible correlation between resistance and underwetting rate and the influence of multiple layers on resistance and wetting rates, but further investigations have to be carried out concerning this possibility. The developed workflow could assist in the investigation of suitable parameters by making sure that the geometrical features of the printed structure are comparable.

The results show that the proposed workflow is suitable for identifying and evaluating each tested parameter variation that influences the wetting behavior without the usage of complex measurement setups. The use of the actual/target comparison for the different track widths has proven to be a useful feature to further evaluate the influence of the wetting behavior and simultaneously give users a first impression of what their tested parameter set is capable of with regard to the layout design. The presented paper might be used as a first step in creating design kits of ink/substrate specific parameters. The workflow might be adopted easily for different printers and be used as the first step in quality control for industrial production. Since the software tool provides elements to compensate for different image types, such as changed substrates or inks, the workflow might also be used to compare different substrate/ink combinations to find the best possible parameters to achieve a high print quality for specific applications.

Author Contributions: Conceptualization, T.H.; methodology, T.H. and H.R.; software, Y.-S.C. and T.H.; validation, T.H., H.R., W.Y. and Y.-S.C.; formal analysis, T.H. and H.R.; investigation, T.H., H.R., W.Y. and Y.-S.C.; resources, K.G. and A.Z.; data curation, T.H., H.R., W.Y. and Y.-S.C.; writing—original draft preparation, T.H. and H.R.; writing—review and editing, W.Y., Y.-S.C., K.G. and A.Z.; visualization, T.H., W.Y. and Y.-S.C.; supervision, T.H. and H.R.; project administration, T.H. All authors have read and agreed to the published version of the manuscript.

Funding: This publication was funded by the German Research Foundation (DFG) grant “Open Access Publishing/2023-2024/University of Stuttgart” (512689491).

Data Availability Statement: All data used are shown in the text. Raw data are available on request.

Conflicts of Interest: The authors declare no conflict of interest.

References

1. Trotter, M.; Juric, D.; Bagherian, Z.; Borst, N.; Gläser, K.; Meissner, T.; von Stetten, F.; Zimmermann, A. Inkjet-Printing of Nanoparticle Gold and Silver Ink on Cyclic Olefin Copolymer for DNA-Sensing Applications. *Sensors* **2020**, *20*, 1333. [CrossRef] [PubMed]
2. Hussin, H.; Soin, N.; Wan Muhamad Hatta, S.F.; Md Rezali, F.A.; Abdul Wahab, Y. Review—Recent Progress in the Diversity of Inkjet-Printed Flexible Sensor Structures in Biomedical Engineering Applications. *J. Electrochem. Soc.* **2021**, *168*, 077508. [CrossRef]
3. Wiklund, J.; Karakoç, A.; Palko, T.; Yiğitler, H.; Ruttik, K.; Jäntti, R.; Paltakari, J. A Review on Printed Electronics: Fabrication Methods, Inks, Substrates, Applications and Environmental Impacts. *J. Manuf. Mater. Process.* **2021**, *5*, 89. [CrossRef]
4. Cinquino, M.; Prontera, C.T.; Zizzari, A.; Giuri, A.; Pugliese, M.; Giannuzzi, R.; Monteduro, A.G.; Carugati, M.; Banfi, A.; Carallo, S.; et al. Effect of Surface Tension and Drying Time on Inkjet-Printed PEDOT:PSS for ITO-Free OLED Devices. *J. Sci. Adv. Mater. Devices* **2021**, *7*, 100394. [CrossRef]
5. Zapka, W. (Ed.) *Handbook of Industrial Inkjet Printing: A Full System Approach*; Wiley-VCH GmbH & Co. KGaA: Weinheim, Germany, 2017; ISBN 9783527687169.
6. Zhou, L.; Chen, X.; Su, W.; Cui, Z.; Lai, W.-Y. In-Depth Investigation of Inkjet-Printed Silver Electrodes over Large-Area: Ink Recipe, Flow, and Solidification. *Adv. Mater. Interfaces* **2022**, *9*, 2102548. [CrossRef]
7. Guo, Y.; Patanwala, H.; Bogner, B.; Ma, A. Inkjet and Inkjet-Based 3D Printing: Connecting Fluid Properties and Printing Performance. *Rapid Prototyp. J.* **2017**, *23*, 562–576. [CrossRef]
8. Zea, M.; Moya, A.; Villa, R.; Gabriel, G. Reliable Paper Surface Treatments for the Development of Inkjet-Printed Electrochemical Sensors. *Adv. Mater. Interfaces* **2022**, *9*, 2200371. [CrossRef]
9. Brishty, F.P.; Urner, R.; Grau, G. Machine Learning Based Data Driven Inkjet Printed Electronics: Jetting Prediction for Novel Inks. *Flex. Print. Electron.* **2022**, *7*, 015009. [CrossRef]
10. Schliske, S.; Rath, S.; Ruiz-Preciado, L.A.; Lemmer, U.; Exner, K.; Hernandez-Sosa, G. Surface Energy Patterning for Ink-Independent Process Optimization of Inkjet-Printed Electronics. *Flex. Print. Electron.* **2021**, *6*, 015022. [CrossRef]
11. Lawrence, J.; Li, L. Modification of the Wettability Characteristics of Polymethyl Methacrylate (PMMA) by Means of CO₂, Nd:YAG, Excimer and High Power Diode Laser Radiation. *Mater. Sci. Eng. A* **2001**, *303*, 142–149. [CrossRef]
12. Hu, S.; Zhu, W.; Yang, W.; Li, M. Morphology Simulation of Drop-on-Demand Inkjet-Printed Droplets. *Npj Flex. Electron.* **2022**, *6*, 64. [CrossRef]
13. Bischoff, P.; Carreiro, A.V.; Kroh, C.; Schuster, C.; Härtling, T. En Route to Automated Maintenance of Industrial Printing Systems: Digital Quantification of Print-Quality Factors Based on Induced Printing Failure. *J. Sens. Sens. Syst.* **2022**, *11*, 277–285. [CrossRef]
14. Arnal, A.; Terés, L.; Ramon, E. Organic and Printed Process Design Kits: Review, Analysis and Comparison. *Flex. Print. Electron.* **2021**, *6*, 033001. [CrossRef]
15. Diaz, E.; Ramon, E.; Carrabina, J. Inkjet Patterning of Multiline Intersections for Wirings in Printed Electronics. *Langmuir* **2013**, *29*, 12608–12614. [CrossRef] [PubMed]
16. Vila, F.; Pallarès, J.; Ramon, E.; Terés, L. A Systematic Study of Pattern Compensation Methods for All-Inkjet Printing Processes. *IEEE Trans. Compon. Packag. Manuf. Technol.* **2016**, *6*, 630–636. [CrossRef]
17. Mashayekhi, M.; Conde, A.; Ng, T.N.; Mei, P.; Ramon, E.; Martinez-Domingo, C.; Alcalde, A.; Terés, L.; Carrabina Bordoll, J. Inkjet Printing Design Rules Formalization and Improvement. *J. Disp. Technol.* **2015**, *11*, 658–665. [CrossRef]
18. Kwon, J.; Baek, S.; Lee, Y.; Tokito, S.; Jung, S. Layout-to-Bitmap Conversion and Design Rules for Inkjet-Printed Large-Scale Integrated Circuits. *Langmuir* **2021**, *37*, 10692–10701. [CrossRef] [PubMed]
19. Brishty, F.P.; Grau, G. Machine Vision Methodology for Inkjet Printing Drop Sequence Generation and Validation. *Flex. Print. Electron.* **2021**, *6*, 035009. [CrossRef]
20. Gengenbach, U.; Ungerer, M.; Koker, L.; Reichert, K.-M.; Stiller, P.; Allgeier, S.; Köhler, B.; Zhu, X.; Huang, C.; Hagenmeyer, V. Automated Fabrication of Hybrid Printed Electronic Circuits. *Mechatronics* **2020**, *70*, 102403. [CrossRef]
21. von Stetten, F.; Kuderer, M.; Gläser, K. *Universelle Mediatorsonden Plattform mit Elektrochemischer Detektion zur Mobilen Point of Care DNA-Diagnostik (Mobi-E)*; Schlussbericht Zu IGF-Vorhaben Nr. 19364N; Hahn-Schickard, Institut für Mikrosystemtechnik Uni Freiburg: Stuttgart, Germany, 2020.
22. Organization for Small & Medium Enterprises and Regional Innovation. Corporate Profile C-INK Co., Ltd. Catalogue. 2018. Available online: https://jgoodtech.smrj.go.jp/en_US/web/page/corp/-/info/JC000000013257/appeal/eng?get-similar-corp-id=JC000000013257&freeWord= (accessed on 22 December 2022).
23. C-INK Co., Ltd. Safety Data Sheet—Drycure Au-J 1010B. 2018. Available online: <https://www.cink.jp/en/data> (accessed on 22 December 2022).
24. Fujifilm Dimatix, Inc. Dimatix Materials Printer DMP-2850 Data Sheet. 2019. Available online: <https://www.fujifilm.com/de/en/business/inkjet-solutions/deposition-products/dmp-2850/support> (accessed on 22 December 2022).
25. Fujifilm Dimatix, Inc. Guidance on How to Use the New Samba Cartridge Product Data Sheet PDS00142—Dimatix Materials Cartridge—Samba Cartridge. 2021. Available online: <http://dimatix-5352080.hs-sites.com/samba-how-to> (accessed on 22 December 2022).
26. Fujifilm Dimatix, Inc. FUJIFILM Dimatix Materials Printer DMP-2800 Series User Manual 2010. Available online: <https://content.ilabsolutions.com/wp-content/uploads/2016/11/DMP-2800-Users-Guide-Version-2.0-6.pdf> (accessed on 22 December 2022).

27. Kaur, G.; Kaur, R. Image De-Noising Using Wavelet Transform and Various Filters. *Int. J. Res. Comput. Sci.* **2012**, *2*, 15–21. [[CrossRef](#)]
28. Image Filtering Using Convolution in OpenCV | LearnOpenCV. 2021. Available online: <https://learnopencv.com/image-filtering-using-convolution-in-opencv/> (accessed on 14 October 2022).
29. Paris, S.; Kornprobst, P.; Tumblin, J.; Durand, F. A Gentle Introduction to Bilateral Filtering and Its Applications. 130. Available online: <https://people.csail.mit.edu/sparis/bf-course> (accessed on 14 October 2022).
30. Bildfilter: Gaußsche Unschärfe. Available online: <https://ichi.pro/de/bildfilter-gaussische-unschaeffe-258620841755057> (accessed on 14 October 2022).
31. Bora, D.J.; Gupta, A.K.; Khan, F.A. Comparing the Performance of L*A*B* and HSV Color Spaces with Respect to Color Image Segmentation. *arXiv* **2015**, arXiv:1506.01472.
32. Otsu, N. A Threshold Selection Method from Gray-Level Histograms. *IEEE Trans. Syst. Man Cybern.* **1979**, *9*, 62–66. [[CrossRef](#)]
33. Ledda, A. *Mathematical Morphology in Image Processing*; Universität Gent: Gent, Belgium, 2007.
34. Smith, S.W. *The Scientist and Engineer's Guide to Digital Signal Processing*, 2nd ed.; California Technical Pub.: San Diego, CA, USA, 1999; ISBN 9780966017670.
35. The Normal Distribution—Sociology 3112—Department of Sociology—The University of Utah. Available online: <https://soc.utah.edu/sociology3112/normal-distribution.php> (accessed on 8 November 2022).

Disclaimer/Publisher's Note: The statements, opinions and data contained in all publications are solely those of the individual author(s) and contributor(s) and not of MDPI and/or the editor(s). MDPI and/or the editor(s) disclaim responsibility for any injury to people or property resulting from any ideas, methods, instructions or products referred to in the content.